Solid State Sciences 180 (2026) 108401

Contents lists available at ScienceDirect

Solid State Sciences

journal homepage: www.elsevier.com/locate/ssscie

An octameric fluoridopalladate(IV) $[Pd_8F_{36}]^{4-}$ anion in KPd_2F_9 revealed by 3D electron diffraction

Klemen Motaln [a,b], Kshitij Gurung [c], Mirela Dragomir [a,b], Lukáš Palatinus [c,*], Matic Lozinšek [a,b,**]

[a] Jožef Stefan Institute, Jamova cesta 39, 1000 Ljubljana, Slovenia
[b] Jožef Stefan International Postgraduate School, Jamova cesta 39, 1000 Ljubljana, Slovenia
[c] Institute of Physics, Academy of Sciences of the Czech Republic, Na Slovance 1999/2, 182 00 Prague 8, Czechia

ARTICLE INFO

Keywords:
Fluorides
Fluoridometallates
Palladium tetrafluoride
Crystal structure
3D electron diffraction
Raman spectroscopy

ABSTRACT

The chemistry of fluoridopalladates(IV) is mainly limited to salts containing the discrete $[PdF_6]^{2-}$ anion. Reaction of K_2PdF_6 with AsF_5 in anhydrous HF results in the removal of KF as $KAsF_6$ and the formation of KPd_2F_9. The product was characterized by Raman spectroscopy, powder X-ray diffraction and 3D electron diffraction (3D ED). Crystal structure elucidation revealed a rare example of an oligomeric fluoridopalladate(IV) anion, namely the cube-shaped octameric $[Pd_8F_{36}]^{4-}$ species. Raman spectroscopic investigations of analogous reactions involving Rb_2PdF_6 and Cs_2PdF_6 indicate that related fluoridopalladate(IV) species also likely formed.

1. Introduction

Palladium tetrafluoride, PdF_4 [1,2], the highest-valent binary fluoride of palladium [3], is a potent oxidizing and fluorinating agent capable, for example, of oxidizing XeF_2 to XeF_4 [4]. As a consequence, the synthesis of pure PdF_4 is somewhat challenging and frequently results in samples contaminated with Pd_2F_6 impurities [5–7]. Fluoridopalladates(IV), the anionic derivatives of the Lewis-acidic PdF_4, are, in contrast, considerably easier to prepare [8], owing to the lower effective electronegativity of the high-oxidation-state metal centre in an anion compared with that in the neutral binary fluoride or in cationic species [9].

The chemistry of fluoridopalladates(IV) is mainly limited to salts containing the discrete $[PdF_6]^{2-}$ anion. These include salts of monovalent cations such as Li_2PdF_6 [10], Na_2PdF_6 [10,11], K_2PdF_6, Rb_2PdF_6, Cs_2PdF_6 [12–14] divalent cation salts including $MgPdF_6$, $CaPdF_6$ [10], $SrPdF_6$, $BaPdF_6$ [15], $NiPdF_6$, $CuPdF_6$ [16], $ZnPdF_6$ [10], $Pd^{II}Pd^{IV}F_6$ [1,16,17], $Ag^{II}Pd^{IV}F_6$ [18], $CdPdF_6$ [10], and $PbPdF_6$ [19]; the trivalent example $La_2(PdF_6)_3$ [20]; as well as salts containing heteroatomic cations, such as $(SeF_3)_2PdF_6$ [14], $[XeF_5]_2[PdF_6]$ [21,22], $[Xe_2F_{11}]_2[PdF_6]$ [22], and $(NO)_2PdF_6$ [22,23].

Only recently was the first example of a polymeric fluoridopalladate (IV) structurally elucidated: the corrugated ladder $[Pd_2F_9]^-$ anion, identified in the crystal structure of $[XeF][Pd_2F_9]$ ($XeF_2{\cdot}2PdF_4$) [5] determined by 3D electron diffraction [7]. The existence of a potassium fluoridopalladate(IV) featuring a complex anion, tentatively formulated as "$KPdF_5$", has previously been proposed on the basis of the formation of an intermediate brown precipitate upon reaction of K_2PdF_6 with excess AsF_5 in anhydrous HF (aHF) [24], as well as the isolation of a yellow–orange solid from reactions of equimolar amounts of K_2PdF_6 with BiF_5 in aHF [25]. However, neither product was characterized in detail.

A major obstacle in attempts to characterize complex fluoridopalladates(IV) arises from their tendency to form powdered products, which, together with the lack of suitable solvents for recrystallization, precludes structural investigation by single-crystal X-ray diffraction (SCXRD). Crystal-structure determination of such samples may nevertheless be achieved by 3D electron diffraction (3D ED), which requires crystallites several orders of magnitude smaller than those needed for SCXRD [26,27]. However, the application of 3D ED to reactive compounds remains comparatively underexplored [7,28,29], although several sample-handling protocols for the structural characterization of sensitive microcrystalline species have recently been successfully demonstrated [30–32]. In addition to ensuring that such

This article is part of a special issue entitled: ECSSC 2025 published in Solid State Sciences.

* Corresponding author.
** Corresponding author. Jožef Stefan Institute, Jamova cesta 39, 1000 Ljubljana, Slovenia.
E-mail addresses: palat@fzu.cz (L. Palatinus), matic.lozinsek@ijs.si (M. Lozinšek).

https://doi.org/10.1016/j.solidstatesciences.2026.108401
Received 23 January 2026; Received in revised form 15 May 2026; Accepted 28 May 2026
Available online 3 June 2026

samples can be transferred into the instrument without decomposition, it must also be established that they neither sublime under the high-vacuum conditions of the microscope nor undergo extensive electron-beam-induced damage [31]. These issues can be mitigated by cooling the sample to cryogenic temperatures during insertion and data acquisition [33,34] and by minimizing the electron dose deposited on the sample [35,36]. Merging incomplete diffraction datasets from several distinct crystallites [37] can further facilitate structure solution in cases where the sample suffers significant radiation damage during the diffraction experiment.

In this work, the synthesis and structural characterization of the novel complex fluoridopalladate(IV) salt KPd_2F_9 are reported. By applying a recently described sample-transfer procedure [30,31], this highly sensitive compound was successfully introduced into a transmission electron microscope (TEM), and its structure was determined by 3D ED. The analysis revealed a cube-like, octameric $[Pd_8F_{36}]^{4-}$ anion, representing the first example of an oligomeric fluoridopalladate(IV) species.

2. Experimental section

Caution: Anhydrous HF (aHF), F_2, and AsF_5 must be handled with great care in a well-ventilated fume hood, and appropriate protective gear must be worn at all times. Experimentalists working with these chemicals must be fully aware of the dangers they pose and have access to appropriate emergency treatment procedures in the event of exposure [38,39].

2.1. General apparatus and techniques

Work involving volatile reagents (aHF, F_2, and AsF_5) was conducted on a custom-built, fluorine-resistant vacuum line constructed from nickel and copper and equipped with PTFE (polytetrafluoroethylene) and FEP (fluorinated ethylene propylene) manifolds. All solids were stored and handled in a nitrogen-filled glovebox (Vigor SG1200/750E–SG1500/750E), with moisture levels maintained below 1 ppm at all times. Syntheses were carried out in h-shaped FEP vessels fitted with brass-encased PTFE valves. Each vessel comprised two arms constructed from 6 mm i.d. (8 mm o.d.) FEP tubing, joined to the valve via a brass-encased PTFE T-section, such that the straight "main" arm was aligned parallel to the valve body, while the angled "side" arm was attached at a right angle. Both reactor arms contained PTFE-coated magnetic stir bars. All reaction vessels were passivated with F_2 prior to use.

2.2. Reagents

KF (Acros Organics, 99.99%), RbF (Alfa-Aesar, 99.975%), CsF (Sigma-Aldrich, 99.9%), and Pd (Aldrich, 99.9%) were used as supplied without further purification. The aHF solvent was dried by treating commercial anhydrous HF (Linde, 99.995 %) with K_2NiF_6 (Advance Research Chemicals, 99.9%) for at least 12 h prior to use. AsF_5 was synthesized by static fluorination of As_2O_3 in a nickel vessel [40]. The K_2PdF_6 starting material was prepared from KF, Pd, and excess F_2 in aHF, following the previously published procedure [8]. Powder X-ray diffraction (PXRD) analysis of the resulting K_2PdF_6 revealed that α-K_2PdF_6 is the predominant phase (90.4(1) wt %), with β-K_2PdF_6 present as a minor phase (9.6(1) wt %) (Fig. S1). The refined unit-cell parameters of α-K_2PdF_6 ($P\bar{3}m1$; $a = 5.7208(4)$ Å, $c = 4.6714(2)$ Å, $V = 132.4(2)$ Å^3) and β-K_2PdF_6 ($P6_3mc$; $a = 5.790(3)$ Å, $c = 9.440(3)$ Å, $V = 274.1(1)$ Å^3) are in good agreement with previously reported room-temperature PXRD data (α-K_2PdF_6: $a = 5.717(3)$ Å, $c = 4.667(3)$ Å, $V = 132.1(2)$ Å^3 [41]; β-K_2PdF_6: $a = 5.7971(2)$ Å, $c = 9.4172(5)$ Å, $V = 274.07(2)$ Å^3 [41]).

2.3. Synthesis of KPd_2F_9

In a typical experiment, KF (41 mg, 0.706 mmol), Pd (35 mg, 0.329 mmol), and excess F_2 were reacted in aHF (1.4 mL) at room temperature [8]. Fluorine was introduced in two portions (0.938 and 0.584 mmol), each followed by 24 h of vigorous stirring. After two days, a bright yellow solution of K_2PdF_6 formed, accompanied by only minor amounts of an insoluble brown precipitate. Unreacted F_2 was then evacuated, and AsF_5 (0.359 mmol) was condensed into the reactor at −196 °C. Upon warming to ambient temperature, a yellow precipitate developed (Eq. 1). After an additional 2 h of stirring, the supernatant was decanted into the "side" arm, and the solvent was recondensed into the "main" arm by cooling with liquid nitrogen, thereby retaining the aHF-soluble byproducts in the "side" arm. Following three such solvent extraction and decantation cycles, the solvent was removed, revealing a sand-brown solid in the "main" arm (Fig. S2) and an off-white material in the "side" arm. The off-white fraction was identified as a mixture mainly of $KAsF_6$ and K_2PdF_6 by Raman spectroscopy and PXRD (Fig. S3).

$$2K_2PdF_6 + 3AsF_5 \rightarrow KPd_2F_9 + 3KAsF_6 \quad \text{(Eq. 1)}$$

2.4. Attempted synthesis of Rb and Cs analogues

The synthetic procedure described for KPd_2F_9 was also applied in attempts to prepare Rb and Cs salts containing complex fluoridopalladate(IV) anions. Rb_2PdF_6 was prepared from RbF (72 mg, 0.689 mmol), Pd (37 mg, 0.348 mmol), and excess F_2 (1.706 mmol, added in two portions) in aHF (1.2 mL), whereas Cs_2PdF_6 was synthesized from CsF (102 mg, 0.671 mmol), Pd (36 mg, 0.338 mmol), and excess F_2 (1.711 mmol, added in two portions) in aHF (1.2 mL). Subsequently, AsF_5 (0.347 mmol and 0.341 mmol, respectively) was introduced into the reactors containing Rb_2PdF_6 and Cs_2PdF_6. In both cases, tan-coloured precipitates formed, slightly darker in the Rb system, and the insoluble fractions were separated from aHF-soluble byproducts by 10 and 12 solvent extraction and decantation cycles, respectively. During purification, the colour of the precipitates gradually darkened, consistent with partial decomposition of the products and formation of Pd_2F_6, the presence of which was confirmed by Raman spectroscopy.

2.5. Characterization

2.5.1. 3D electron diffraction

3D ED measurements were performed on a Tecnai G^2 TEM equipped with a LaB_6 electron source operated at 200 kV (λ = 0.02508 Å). Data were collected at 100 K using a continuous-rotation electron diffraction method over a tilt range of −60° to +60°, with a tilt step of 0.30° per frame. Diffraction patterns were recorded using a Medipix3 hybrid pixel detector (ASI CheeTah) with a resolution of 512 × 512 pixels, a 24-bit dynamic range, and a pixel size of 55 × 55 μm.

Although KPd_2F_9 is highly air-sensitive and very reactive, typically decomposing within less than an hour even when handled in a glovebox using rigorously dried equipment such as metal spatula and agate mortar, the sample was successfully introduced into the TEM for 3D ED measurements by employing a recently developed sample handling and transfer procedure [30,31]. Following this procedure, the FEP ampoule containing the sample was cut open in an N_2-filled glovebox, and the microcrystalline powder was poured onto a Mo TEM grid preloaded in a precooled (<−150 °C) Gatan Model 914 cryotransfer holder, which was then rapidly transferred into the TEM column.

Data sets from two different crystallites (Fig. 1) were merged and processed using *PETS2* software [42] and subsequently imported into *Jana2020* [43] for structure solution using *Superflip* [44]. The structures were initially refined kinematically and, without further optimization of the kinematical refinement, were subsequently refined dynamically [45,

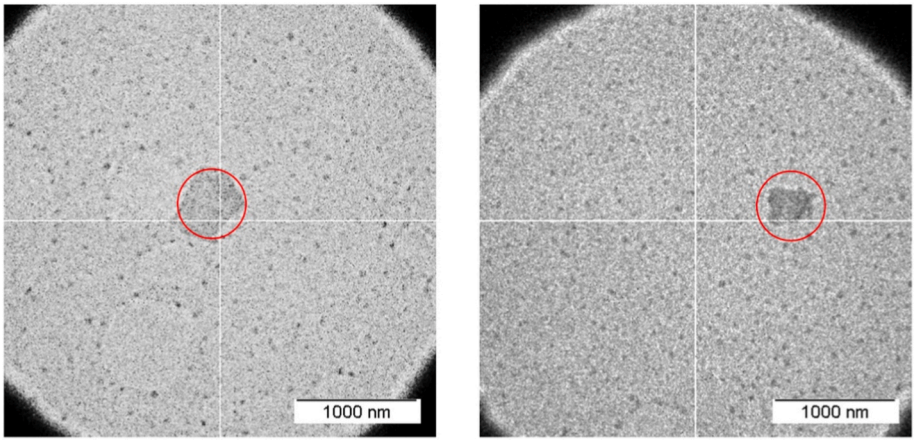

Fig. 1. TEM images of submicron-sized crystallites of KPd_2F_9 used for 3D ED measurements. The red circles indicate the electron beam size. (For interpretation of the references to colour in this figure legend, the reader is referred to the Web version of this article.)

46].

Diffraction patterns were indexed in the monoclinic space group *I2/a* (Table 1). Reciprocal-space reconstructions (Fig. 2) confirmed *I*-centering (*hk*0: $h + k = 2n$; 1*kl*: $k + l = 2n + 1$) and the presence of an *a*-glide (*h*0*l*: $h = 2n + 1$ absences), fully consistent with *I2/a*. The merged data set reached 90.0% completeness, and the apparent mosaicities, determined by resolution-dependent fitting of the rocking curves, were 0.189° and 0.116°. For the refinements, a resolution cutoff of $\sin(\theta_{max})/\lambda = 0.70$ Å^{-1} was applied, and after dynamical refinement, the *R* values converged to $R_{obs} = 0.0790$, $wR_{obs} = 0.0781$, $R_{all} = 0.1470$, and $wR_{all} = 0.0856$.

2.5.2. Raman spectroscopy

Raman spectra were acquired at −173 °C using a Bruker Senterra II confocal Raman microscope equipped with a Linkam LTS420 low-temperature stage. Spectra were collected over the 50–1410 cm^{-1} range at a resolution of 1.5 cm^{-1}, using a 15×1000 μm^2 aperture for KPd_2F_9 and a 50×1000 μm^2 aperture for the Rb and Cs compounds. Samples were excited with a 785 nm laser operated at 25 mW for KPd_2F_9 and the Cs compound and at 10 mW for the Rb compound. Background subtraction was performed using the Bruker *OPUS* 8.7 software suite, applying three iterations of concave rubber-band correction with 64 baseline points. Prior to analysis, samples were loaded into thoroughly dried, F_2-passivated quartz capillaries, which were subsequently flame-sealed in a hydrogen–oxygen flame.

Table 1
3D ED measurement parameters, crystal structure and refinement details.

Measurement parameters	
3D ED collection method	Continuous-rotation data collection from two crystallites
Tilt information α_{min}, α_{max}, $\Delta\alpha$ [°]	−60, +60, 0.30
Exposure time [ms]	504
Beam diameter [nm]	565
Camera length [mm]	1500
Crystal information	
Empirical formula	KPd_2F_9
Formula unit, *Z*	16
Space group	*I2/a*
a, *b*, *c* [Å]	17.8220(8), 9.6213(10), 18.1213(7)
α, β, γ [°]	90, 116.127(3), 90
V [Å^3]	2789.8(3)
Apparent mosaicities [°]	0.189, 0.116
Completeness [%]	90.0
Dynamical refinement	
$\sin(\theta_{max})/\lambda$ [Å^{-1}]	0.70
N_{obs}, N_{all}	6549, 19109
Number of parameters	345
R_{obs}, wR_{obs}	0.0790, 0.0781
R_{all}, wR_{all}	0.1470, 0.0856
$\Delta V(r)_{min}$, $\Delta V(r)_{max}$ [e Å^{-1}]	−0.50, 0.90

2.5.3. Powder X-ray diffraction

PXRD patterns were measured at ambient temperature on a Rigaku OD XtaLAB Synergy-S diffractometer equipped with a Dectris EIGER2 R CdTe 1M detector, using microfocused Ag Kα radiation (λ = 0.56087 Å). Measurement parameters were identical to those previously reported [7, 47], and the final profiles were extracted and processed using *CrysAlisPro* software [48]. Measurements were performed on samples sealed in quartz capillaries prepared as described above. Structure refinements and quantitative phase analyses using the Rietveld refinement method were performed with the *GSAS-II* software [49].

3. Results and discussion

3.1. Crystal structure

KPd_2F_9 crystallizes in the monoclinic space group *I2/a* with $Z' = 2$ and $Z = 16$ (Fig. 3). The two crystallographically distinct K^+ cations, K1 and K2, are coordinated by 9 and 11 fluoride ligands, respectively, resulting in an irregular coordination environment, with the K−F distances spanning a wide range of values (2.626(4)–3.178(5) Å for K1 and 2.720(3)–3.162(5) Å for K2). Owing to the large number of K···F contacts with distances shorter than the sum of the van der Waals radii (4.19 Å; F: 1.46 Å; K: 2.73 Å) [50], only the contacts up to 3.2 Å are tabulated (Table 2) and depicted (Fig. 4), as the corresponding bond-valence sums amount to 1.00 and 1.03 for K1 and K2, respectively (Table S1; $R_0 = 1.992$ Å, $B = 0.37$ Å [51]).

The $[Pd_8F_{36}]^{4-}$ anion is composed of eight $[PdF_6]$ units, each linked to three neighbouring units through three *fac*-arranged fluoride ligands, resulting in an octameric, cube-like motif (Fig. 5). This assembly can also be described as two stacked, puckered tetrameric rings, whose conformation is analogous to those observed in RuF_5 [52], RhF_5 [53], and $XeF_2{\cdot}MnF_4$ [30], with one ring rotated by approximately a right angle relative to the other. A related tetrameric ring motif is also present in $[XeF]^+[Pd_2F_9]^-$ ($XeF_2{\cdot}2PdF_4$) [7], where such four-membered rings are connected to two adjacent rings to form a corrugated ladder-like arrangement.

The Pd−F−Pd angles around the bridging fluoride ligands in KPd_2F_9 (130.2(3)–134.6(4)°) closely match those observed in $[XeF][Pd_2F_9]$ (132.0(3)–134.4(3)°). These angles are substantially less obtuse than the corresponding Ti−F−Ti angles in the cube-like $[Ti_8F_{36}]^{4-}$ anions found in $K_4Ti_8F_{36}{\cdot}8HF$ (155.63(13)–172.20(12)°) and $Rb_4Ti_8F_{36}{\cdot}6HF$ (159.8

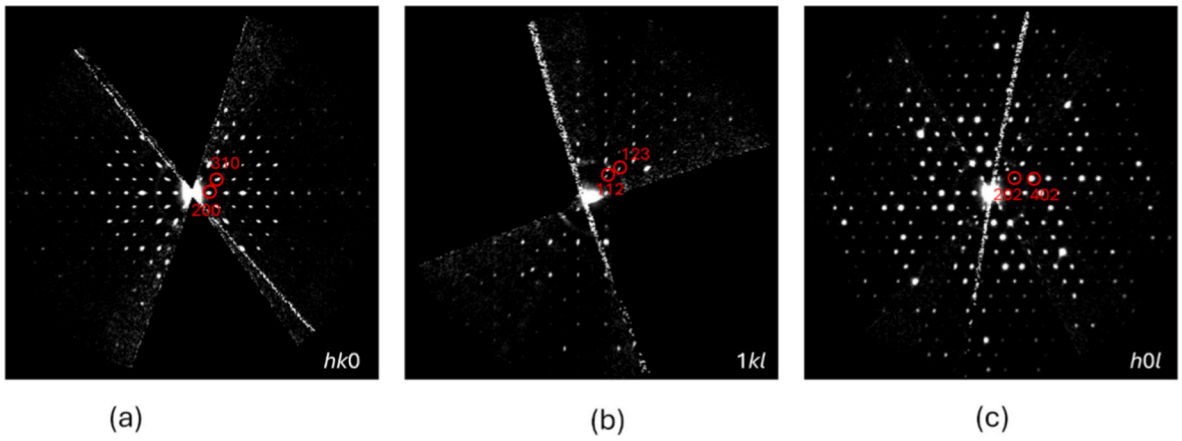

Fig. 2. Reciprocal space reconstructions of KPd_2F_9: (a) The *hk*0 section shows reflections only for $h + k = 2n$, consistent with *I*-centering. (b) The 1*kl* section, in which the reflection pattern is offset by one index in *k* ($k + l = 2n + 1$), further confirms the body-centered (*I*) lattice. (c) The *h*0*l* section reveals systematic absences for $h = 2n + 1$, confirming the presence of an *a*-glide plane. Taken together, these reflection conditions ($h + k + l = 2n$ and *h*0*l*, $h = 2n$) uniquely identify the space group as *I*2/*a* (No. 15).

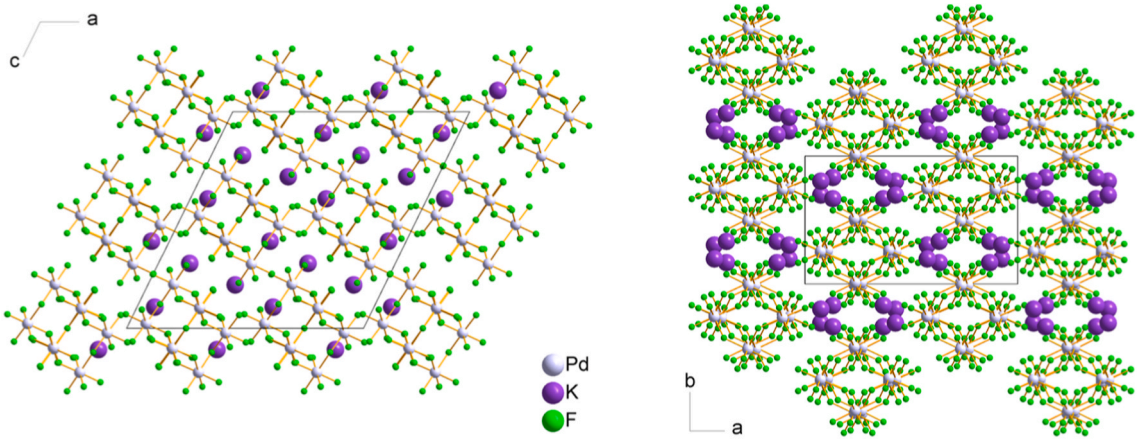

Fig. 3. Crystal packing and the unit cell of the KPd_2F_9 crystal structure viewed along the crystallographic *b*- (left) and *c*-axis (right).

(4)–176.5(4)°) [54], resulting in a more strongly puckered cube-like structure of $[Pd_8F_{36}]^{4-}$.

The geometries of the individual $[PdF_6]$ units deviate from octahedral symmetry, as reflected by deviations of the *cis*-F−Pd−F (87.1(2)–93.33(18)°) and *trans*-F−Pd−F angles (177.11(19)–179.9(2)°) from the ideal values. The shorter terminal Pd−F_t bonds (1.825(4)–1.872(5) Å) and the longer bridging Pd−F_b(Pd) bonds (1.951(4)–2.000(3) Å) are comparable to those observed for the corrugated ladder-like $[Pd_2F_9]^-$

Table 2
Selected bond distances and angles in the crystal structure of KPd_2F_9.

Bond distances [Å]							
K1−F2^{i}	3.178(5)	K1−F11^{iii}	2.626(4)	K2−F1^{vi}	2.934(6)	K2−F12	2.940(6)
K1−F3^{ii}	2.739(4)	K1−F13^{iv}	2.833(5)	K2−F2^{v}	2.965(5)	K2−F12^{vii}	2.817(3)
K1−F6^{ii}	3.082(4)	K1−F17^{v}	2.780(4)	K2−F2^{vi}	3.162(5)	K2−F13^{vii}	2.862(4)
K1−F7^{ii}	3.038(6)	K1−F18^{v}	2.735(4)	K2−F3^{vi}	2.795(4)	K2−F17^{vii}	2.858(6)
K1−F9	2.633(5)			K2−F7^{iii}	2.720(3)	K2−F18^{iv}	2.834(5)
				K2−F8^{iii}	2.819(4)		
Pd1−F1	1.830(5)	Pd2−F5	1.982(3)	Pd3−F10	1.984(4)	Pd4−F4	1.994(5)
Pd1−F2	1.836(5)	Pd2−F7	1.831(5)	Pd3−F11	1.825(4)	Pd4−F14	1.983(4)
Pd1−F3	1.855(4)	Pd2−F8	1.840(4)	Pd3−F12	1.851(5)	Pd4−F16	1.864(4)
Pd1−F4	1.951(4)	Pd2−F9	1.853(4)	Pd3−F13	1.863(4)	Pd4−F17	1.872(5)
Pd1−F5	1.952(4)	Pd2−F10	1.954(5)	Pd3−F14	1.959(4)	Pd4−F18	1.864(4)
Pd1−F6	2.000(3)	Pd2−F19	1.996(4)	Pd3−F15	1.980(3)	Pd4−F19^{viii}	1.979(4)
Bond angles [°]							
Pd1−F5−Pd2	132.6(2)	Pd2−F10−Pd3	132.5(2)	Pd3−F15−Pd3^{viii}	131.7(4)		
Pd1−F4−Pd4	131.1(2)	Pd2−F19−Pd4^{viii}	130.2(3)	Pd3−F14−Pd4	131.7(2)		
Pd1−F6−Pd1^{viii}	134.6(4)						

Symmetry codes: (i) $x - 1/2, -y + 2, z$; (ii) $-x + 1, -y + 2, -z + 1$; (iii) $-x + 1, -y + 1, -z + 1$; (iv) $x - 1/2, -y + 1, z$; (v) $-x + 3/2, -y + 3/2, -z + 3/2$; (vi) $x, y - 1, z$; (vii) $-x + 3/2, -y + 1/2, -z + 3/2$; (viii) $-x + 3/2, y, -z + 1$.

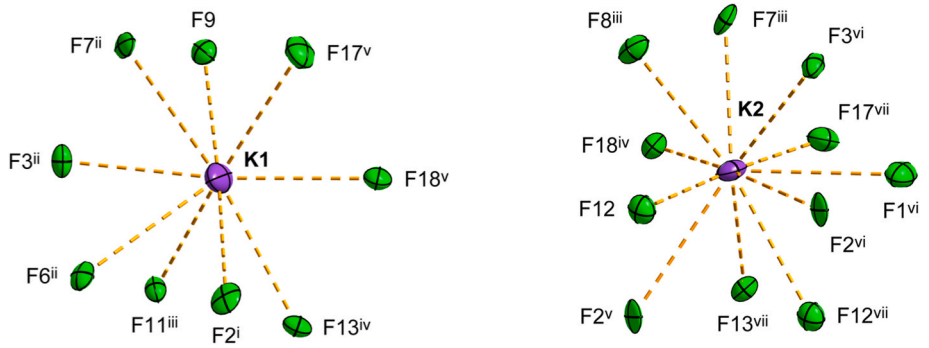

Fig. 4. Coordination environments of the two crystallographically independent K^+ cations in KPd_2F_9. Displacement ellipsoids are depicted at the 50% probability level.

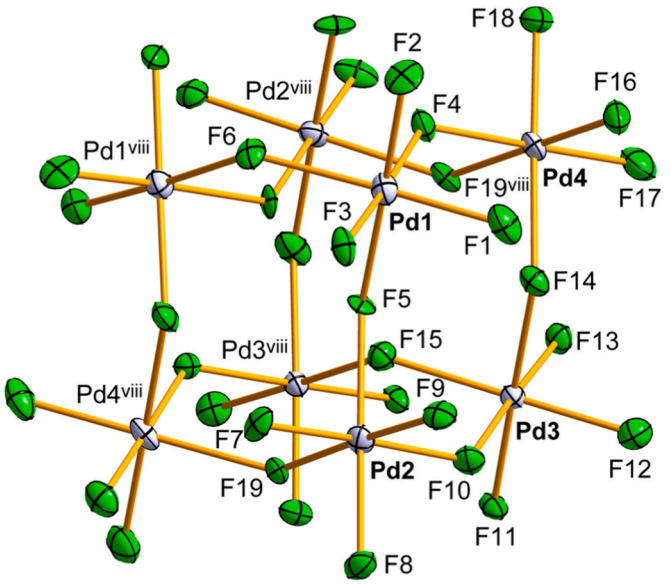

Fig. 5. Puckered, cube-like oligomeric $[Pd_8F_{36}]^{4-}$ anion in KPd_2F_9, shown with the atom-numbering scheme. Displacement ellipsoids are depicted at the 50% probability level.

anion in the structure of $[XeF][Pd_2F_9]$ (Pd−F_t: 1.844(4)–1.866(4) Å; Pd−F_b(Pd): 1.946(4)–2.020(4) Å) [7], as well as those reported for the $[PdF_3(XeF_2)_3]^+$ adduct cation in the double salt $[Xe_2F_3][PdF_3(XeF_2)_3][AsF_6]_2$ (Pd−F_t: 1.842(5)–1.860(4) Å; Pd−F_b(Xe): 1.975(4)–1.990(4) Å) [55]. These values also bracket the Pd−F bond distances exhibited by the discrete $[PdF_6]^{2-}$ anions in the structures of α-K_2PdF_6 (1.8974(13) Å), β-K_2PdF_6 (1.892(4) Å) [41], and $[XeF_5]_2^+[PdF_6]^{2-}$ (1.860(6)–1.902 (7) Å) [21].

3.2. Raman spectroscopy

The low-temperature (−173 °C) Raman spectrum of KPd_2F_9 (Fig. 6, Table S2) exhibits the most intense bands in the 620–670 cm^{-1} region. The positions of these features, attributable to Pd−F_t stretching modes, are markedly blue-shifted relative to the ν_1 vibration of the discrete $[PdF_6]^{2-}$ anion, which is typically observed at 558–575 cm^{-1} [20]. A similar trend has been reported for fluoridotitanates(IV), in which the strong Ti−F_t stretching bands of oligo- and polymeric anions occur between those of $[TiF_6]^{2-}$ and solid TiF_4 and shift to higher frequencies as the charge/TiF_4 ratio increases [54,56,57]. The Raman spectrum of the only crystallographically characterized polymeric fluoridopalladate(IV) to date, $[XeF][Pd_2F_9]$, likewise shows three prominent bands in the 630–660 cm^{-1} range, with the most intense peak at 653 cm^{-1} [7].

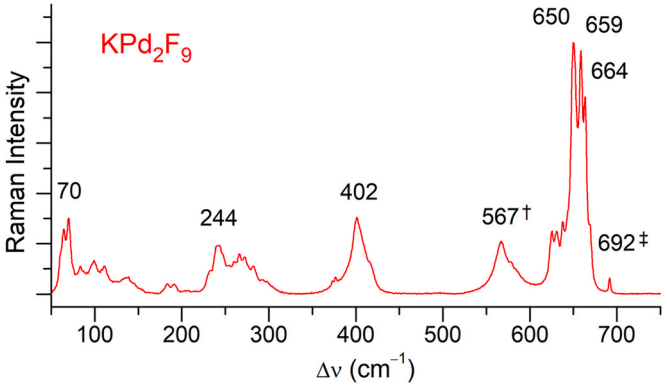

Fig. 6. Low-temperature (−173 °C) Raman spectrum of KPd_2F_9. Peaks arising from impurities are labelled by † (Pd_2F_6) and ‡ ($KAsF_6$).

Collectively, these observations highlight Raman spectroscopy as an effective tool for rapid and reliable identification of polymeric and oligomeric fluoridopalladate(IV) compounds. The spectrum also reveals the presence of two impurities, Pd_2F_6 and $KAsF_6$, identified by their

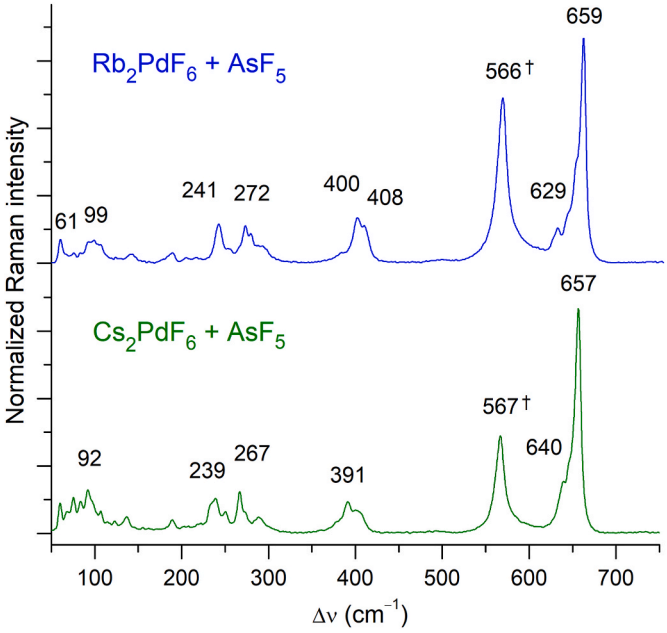

Fig. 7. Low-temperature (−173 °C) Raman spectra of the products formed upon interaction of AsF_5 with Rb_2PdF_6 (top) and Cs_2PdF_6 (bottom). Peaks originating from Pd_2F_6 are labelled by †.

strong octahedral ν_1 modes at 567 and 692 cm^{-1}, respectively [20,58].

Raman spectra of the tan-coloured products obtained upon addition of an equimolar amount of AsF_5 to aHF solutions containing either Rb_2PdF_6 or Cs_2PdF_6 indicate the formation of products featuring oligomeric or polymeric fluoridopalladate(IV) anions (Fig. 7, Table S2). The positions of the most intense bands in the spectra of the rubidium (659 cm^{-1}) and caesium systems (657 cm^{-1}) are consistent with vibrations associated with fluoridopalladate(IV) anions in $[XeF][Pd_2F_9]$ (653 cm^{-1}) [7] and KPd_2F_9 (650–664 cm^{-1}). However, the absence of complementary structural information for these poorly crystalline phases precludes definitive identification of the products.

4. Conclusions

The extraction of KF from K_2PdF_6 by AsF_5 in aHF results in the formation of KPd_2F_9. The resulting microcrystalline powder was characterized by PXRD and low-temperature Raman spectroscopy. The crystal structure of KPd_2F_9 was elucidated by 3D electron diffraction measured on submicron crystallites. The octameric, cube-shaped $[Pd_8F_{36}]^{4-}$ anion constitutes the first example of an oligomeric fluoridopalladate(IV) species. Preliminary investigations of analogous reactions involving Rb_2PdF_6 and Cs_2PdF_6 suggest that oligomeric or polymeric fluoridopalladate(IV) anions are likewise formed. These results demonstrate that anionic fluoridopalladate(IV) species could exhibit a level of structural diversity comparable to that observed in other families of fluoridometallate(IV) salts [59] derived from the corresponding metal tetrafluorides. Furthermore, the successful cryotransfer of air-sensitive KPd_2F_9 into the TEM, together with the subsequent crystal structure elucidation, confirms the applicability of this sample-transfer procedure [30,31] and the 3D ED technique for the analysis of strongly oxidizing, high-valent metal compounds.

CRediT authorship contribution statement

Klemen Motaln: Conceptualization, Data curation, Formal analysis, Investigation, Validation, Visualization, Writing – original draft, Writing – review & editing. **Kshitij Gurung:** Data curation, Formal analysis, Investigation, Validation, Visualization, Writing – original draft, Writing – review & editing. **Mirela Dragomir:** Formal analysis, Validation, Visualization, Writing – review & editing. **Lukáš Palatinus:** Funding acquisition, Project administration, Resources, Supervision, Writing – review & editing. **Matic Lozinšek:** Funding acquisition, Project administration, Resources, Supervision, Validation, Visualization, Writing – original draft, Writing – review & editing.

Declaration of competing interest

The authors declare that they have no known competing financial interests or personal relationships that could have appeared to influence the work reported in this paper.

Acknowledgements

Financial support from the Slovenian Research and Innovation Agency (ARIS) (N1-0189) and the Czech Science Foundation (GACR) (21-06744K) in the form of joint project (GACR–ARIS) within the Central European Science Partnership (CEUS), the European Research Council (ERC) under the European Union's Horizon 2020 Research and Innovation Programme (Starting Grant No. 950625), and the Jožef Stefan Institute Director's Fund is gratefully acknowledged. Electron diffraction experiments were performed within the CzechNanoLab Research Infrastructure and the Terafit project, both supported by the Ministry of Education, Youth and Sports of the Czech Republic (MEYS CR) (project numbers LM2023051 and CZ.02.01.01/00/22_008/0004594).

Appendix A. Supplementary data

Supplementary data to this article can be found online at https://doi.org/10.1016/j.solidstatesciences.2026.108401.

Data availability

Data for this article, including 3D ED dataset, PXRD data, and Raman spectra is available at Zenodo open repository at https://doi.org/10.5281/zenodo.18430079. CSD 2525417 contains the supplementary crystallographic data for this paper. This data can be obtained free of charge from FIZ Karlsruhe via www.ccdc.cam.ac.uk/structures.

References

[1] N. Bartlett, P.R. Rao, New fluorides of palladium: palladium(II) hexafluoropalladate(IV) and related compounds and palladium tetrafluoride, Proc. Chem. Soc. (1964) 393–394, https://doi.org/10.1039/PS9640000385.
[2] P.R. Rao, A. Tressaud, N. Bartlett, The tetrafluorides of iridium, rhodium and palladium, J. Inorg. Nucl. Chem. 28 (Supplement) (1976) 23–28, https://doi.org/10.1016/0022-1902(76)80588-X.
[3] B. Žemva, High oxidation state transition metal fluorides, in: T. Nakajima, B. Žemva, A. Tressaud (Eds.), Advanced Inorganic Fluorides: Synthesis, Characterization and Applications, Elsevier Science, 2000, pp. 79–115.
[4] L. Graham, O. Graudejus, N.K. Jha, N. Bartlett, Concerning the nature of $XePtF_6$, Coord. Chem. Rev. 197 (1) (2000) 321–334, https://doi.org/10.1016/S0010-8545(99)00190-3.
[5] N. Bartlett, B. Žemva, L. Graham, Redox reactions in the XeF_2/platinum fluoride and XeF_2/palladium fluoride systems and the conversion of XeF_2 to XeF_4 and Xe, J. Fluorine Chem. 7 (1–3) (1976) 301–320, https://doi.org/10.1016/S0022-1139(00)84003-8.
[6] Z. Mazej, K. Lutar, B. Žemva, Novel syntheses of some binary fluorides: the role of anhydrous hydrogen fluoride, Acta Chim. Slov. 46 (2) (1999) 229–238.
[7] K. Motaln, K. Gurung, M. Dragomir, D. Kurzydłowski, L. Palatinus, M. Lozinšek, Crystal structures of $XeF_2{\cdot}2PtF_4$ and $XeF_2{\cdot}2PdF_4$ determined by 3D electron diffraction and structural models of $XePtF_6$, Inorg. Chem. 64 (29) (2025) 14968–14976, https://doi.org/10.1021/acs.inorgchem.5c01740.
[8] G.M. Lucier, S.H. Elder, L. Chacon, N. Bartlett, The room temperature oxidation of gold, ruthenium, osmium, iridium, platinum, or palladium with fluorine in anhydrous hydrogen fluoride, Eur. J. Solid State Inorg. Chem. 33 (9) (1996) 809–820.
[9] B. Žemva, N. Bartlett, The room temperature preparation of metastable fluorides and potent oxidizers, J. Fluorine Chem. 127 (11) (2006) 1463–1466, https://doi.org/10.1016/j.jfluchem.2006.09.017.
[10] H. Henkel, R. Hoppe, Neue Ternäre Fluoride des Palladiums und Platins, Z. Anorg. Allg. Chem. 359 (3–4) (1968) 160–177, https://doi.org/10.1002/zaac.19683590305.
[11] B. Cox, D.W.A. Sharp, A.G. Sharpe, Complex fluorides. Part V. Complexes formed by molybdenum hexafluoride, tungsten hexafluoride, and rhodium tetrafluoride, J. Chem. Soc. (1956) 1242–1244, https://doi.org/10.1039/JR9560001242.
[12] A.G. Sharpe, The chemistry of the platinum metals. Part II. Fluoropalladates and fluoroplatinates, J. Chem. Soc. (1953) 197–199, https://doi.org/10.1039/JR9530000197.
[13] R. Hoppe, W. Klemm, Über Fluorokomplexe des Palladiums und des Goldes, Z. Anorg. Allg. Chem. 268 (4–6) (1952) 364–371, https://doi.org/10.1002/zaac.19522680415.
[14] N. Bartlett, J.W. Quail, The preparation of palladium difluoride and complex fluorides of palladium in selenium tetrafluoride, J. Chem. Soc. (1961) 3728–3732, https://doi.org/10.1039/JR9610003728.
[15] B. Cox, Complex fluorides. Part IV. The structural chemistry of complex fluorides of the general formula ABF_6, J. Chem. Soc. (1956) 876–878, https://doi.org/10.1039/JR9560000876.
[16] A. Tressaud, N. Bartlett, Preparation, magnetic properties, and pressure-induced transitions of some $M^{II}M^{IV}F_6$ (M^{II} = Ni, Pd, Cu; M^{IV} = Pd, Pt, Sn) complex fluorides, J. Solid State Chem. 162 (2) (2001) 333–340, https://doi.org/10.1006/jssc.2001.9331.
[17] S. Olszewska, S.B. Pillai, D. Upadhyay, K. Zdun, J. Drapała, K. Motaln, M. Dragomir, M. Lozinšek, D. Kurzydłowski, Pressure-Induced comproportionation in palladium trifluoride, Inorg. Chem. 64 (18) (2025) 9026–9034, https://doi.org/10.1021/acs.inorgchem.5c00465, and references therein.
[18] O. Graudejus, S.H. Elder, G.M. Lucier, C. Shen, N. Bartlett, Room temperature syntheses of AuF_6^- and PtF_6^- Salts, $Ag^+AuF_6^-$, $Ag^{2+}PtF_6^{2-}$, and $Ag^{2+}PdF_6^{2-}$, and an estimate for $E(MF_6^-)$ [M = Pt, Pd], Inorg. Chem. 38 (10) (1999) 2503–2509, https://doi.org/10.1021/ic981397z.
[19] B.G. Müller, Fluorides of copper, silver, gold, and palladium, Angew Chem. Int. Ed. Engl. 26 (11) (1987) 1081–1097, https://doi.org/10.1002/anie.198710811.
[20] Z. Mazej, K. Lutar, Metathetical synthesis of $La_2(PdF_6)_3$ and the vibrational spectra of the PdF_6^{2-} anion, J. Fluorine Chem. 107 (1) (2001) 63–69, https://doi.org/10.1016/S0022-1139(00)00347-X.
[21] K. Leary, D.H. Templeton, A. Zalkin, N. Bartlett, Crystal structure of $[XeF_5^+]_2[PdF_6^{2-}]$, Inorg. Chem. 12 (8) (1973) 1726–1730, https://doi.org/10.1021/ic50126a004.

[22] K. Leary, A. Zalkin, N. Bartlett, Crystal structure of $Xe_2F_{11}^+AuF_6^-$ and the Raman spectrum of $Xe_2F_{11}^+$, Inorg. Chem. 13 (4) (1974) 775–779, https://doi.org/10.1021/ic50134a003.

[23] W.A. Sunder, A.L. Wayda, D. DiStefano, W.E. Falconer, J.E. Griffiths, Syntheses and Raman spectra of nitrosyl fluorometallate salts, J. Fluorine Chem. 14 (4) (1979) 299–325, https://doi.org/10.1016/S0022-1139(00)82974-7.

[24] G.M. Lucier, C. Shen, S.H. Elder, N. Bartlett, Facile routes to NiF_6^{2-}, AgF_4^-, AuF_6^-, and PtF_6^- salts using O_2^+ as a source of O_2F in anhydrous HF, Inorg. Chem. 37 (15) (1998) 3829–3834, https://doi.org/10.1021/ic971603n.

[25] G.M. Lucier, Synthesis, Structure, and Reactivity of High Oxidation State Silver Fluorides and Related Compounds, University of California, Berkeley, 1995. Ph.D. dissertation.

[26] M. Gemmi, E. Mugnaioli, T.E. Gorelik, U. Kolb, L. Palatinus, P. Boullay, S. Hovmöller, J.P. Abrahams, 3D electron diffraction: the nanocrystallography revolution, ACS Cent. Sci. 5 (8) (2019) 1315–1329, https://doi.org/10.1021/acscentsci.9b00394.

[27] T. Gruene, J.J. Holstein, G.H. Clever, B. Keppler, Establishing electron diffraction in chemical crystallography, Nat. Rev. Chem 5 (2021) 660–668, https://doi.org/10.1038/s41570-021-00302-4.

[28] C.G. Jones, M. Asay, L.J. Kim, J.F. Kleinsasser, A. Saha, T.J. Fulton, K.R. Berkley, D. Cascio, A.G. Malyutin, M.P. Conley, B.M. Stoltz, V. Lavallo, J.A. Rodríguez, H. M. Nelson, Characterization of reactive organometallic species via MicroED, ACS Cent. Sci. 5 (9) (2019) 1507–1513, https://doi.org/10.1021/acscentsci.9b00403.

[29] L.R. Doyle, E.A. Thompson, A.L. Burnage, A.C. Whitwood, H.T. Jenkins, S. A. Macgregor, A.S. Weller, MicroED characterization of a robust cationic σ-alkane complex stabilized by the $[B(3,5\text{-}(SF_5)_2C_6H_3)_4]^-$ anion, via on-grid solid/gas single-crystal to single-crystal reactivity, Dalton Trans. 51 (9) (2022) 3661–3665, https://doi.org/10.1039/D2DT00335J.

[30] K. Motaln, K. Gurung, P. Brazda, A. Kokalj, K. Radan, M. Dragomir, B. Žemva, L. Palatinus, M. Lozinšek, Reactive noble-gas compounds explored by 3D electron diffraction: XeF_2–MnF_4 adducts and a facile sample handling procedure, ACS Cent. Sci. 10 (9) (2024) 1733–1741, https://doi.org/10.1021/acscentsci.4c00815.

[31] K. Gurung, E. Uran, K. Motaln, P. Brazda, K. Radan, M. Lozinšek, L. Palatinus, A simple cryotransfer method for 3D electron diffraction measurements of highly sensitive samples, J. Appl. Crystallogr. 58 (3) (2025) 1079–1084, https://doi.org/10.1107/S1600576725002456.

[32] J. Xu, V. Srinivas, R. Kumar, L. Pacoste, Y. Guo, T. Yang, C.C. Sun, M. Högbom, X. Zou, H. Xu, Unveiling the structure of anhydrous sodium valproate with 3D electron diffraction and a facile sample preparation workflow, ACS Cent. Sci. 11 (6) (2025) 960–966, https://doi.org/10.1021/acscentsci.5c00412.

[33] K.-N. Truong, S. Ito, J.M. Wojciechowski, C.R. Göb, C.J. Schürmann, A. Yamano, M.D. Campo, E. Okunishi, Y. Aoyama, T. Mihira, N. Hosogi, J. Benet-Buchholz, E. C. Escudero-Adán, F.J. White, J.D. Ferrara, R. Bücker, Making the most of 3D electron diffraction: best practices to handle a new tool, Symmetry 15 (8) (2023) 1555, https://doi.org/10.3390/sym15081555.

[34] E. Yörük, P. Naumov, Effects of Electron beam damage to crystalline samples: a review, Small Methods 10 (1) (2026) e01584, https://doi.org/10.1002/smtd.202501584.

[35] H. Klein, E. Yörük, S. Kodjikian, Structure solution and refinement of beam-sensitive nano-crystals, Micron 181 (2024) 103634, https://doi.org/10.1016/j.micron.2024.103634.

[36] E. Yörük, C. Lecourt, D. Housset, Y. Izumi, W.L. Ling, S. Kodjikian, E. Tretyakov, K. Inoue, K. Maryunina, C. Desroches, H. Klein, D. Luneau, Electron diffraction unveils the 2D metal-radical framework of two molecule-based magnets, Inorg. Chem. Front. 12 (1) (2024) 328–341, https://doi.org/10.1039/D4QI02257B.

[37] S. Smeets, W. Wan, Serial electron crystallography: merging diffraction data through rank aggregation, J. Appl. Crystallogr. 50 (3) (2017) 885–892, https://doi.org/10.1107/S1600576717005854.

[38] D. Peters, R. Miethchen, Symptoms and treatment of hydrogen fluoride injuries, J. Fluorine Chem. 79 (2) (1996) 161–165, https://doi.org/10.1016/S0022-1139(96)03484-7.

[39] M. Möbs, F. Kraus, Tips and procedures for safe handling of anhydrous hydrogen fluoride and pure elemental fluorine in chemical university laboratories, ACS Chem. Health Saf. 32 (5) (2025) 662–672, https://doi.org/10.1021/acs.chas.5c00117.

[40] Z. Mazej, B. Žemva, Synthesis of arsenic pentafluoride by static fluorination of As_2O_3 in a closed system, J. Fluorine Chem. 126 (9) (2005) 1432–1434, https://doi.org/10.1016/j.jfluchem.2005.07.010.

[41] S.I. Ivlev, A.V. Malin, A.J. Karttunen, R.V. Ostvald, F. Kraus, Reactions of $KBrF_4$ with platinum metals, J. Fluorine Chem. 218 (2019) 11–20, https://doi.org/10.1016/j.jfluchem.2018.11.010.

[42] L. Palatinus, P. Brázda, M. Jelínek, J. Hrdá, G. Steciuk, M. Klementová, Specifics of the data processing of precession electron diffraction tomography data and their implementation in the program *PETS2.0*, Acta Crystallogr. B75 (2019) 512–522, https://doi.org/10.1107/S2052520619007534.

[43] V. Petříček, L. Palatinus, J. Plášil, M. Dušek, JANA2020 – a new version of the crystallographic computing system JANA, Z. Kristallogr. Cryst. Mater. 238 (7–8) (2023) 271–282, https://doi.org/10.1515/zkri-2023-0005.

[44] L. Palatinus, G. Chapuis, *SUPERFLIP* – a computer program for the solution of crystal structures by charge flipping in arbitrary dimensions, J. Appl. Crystallogr. 40 (2007) 786–790, https://doi.org/10.1107/S0021889807029238.

[45] L. Palatinus, V. Petříček, C.A. Corrêa, Structure refinement using precession electron diffraction tomography and dynamical diffraction: theory and implementation, Acta Crystallogr. A71 (2015) 235–244, https://doi.org/10.1107/S2053273315001266.

[46] L. Palatinus, C.A. Corrêa, G. Steciuk, D. Jacob, P. Roussel, P. Boullay, M. Klementová, M. Gemmi, J. Kopeček, M.C. Domeneghetti, F. Cámara, V. Petříček, Structure refinement using precession electron diffraction tomography and dynamical diffraction: tests on experimental data, Acta Crystallogr. B71 (2015) 740–751, https://doi.org/10.1107/S2052520615017023.

[47] M. Belak Vivod, Z. Jagličić, G. King, T.C. Hansen, M. Lozinšek, M. Dragomir, Mechanochemical synthesis and magnetic properties of the mixed-valent binary silver(I,II) fluorides, $Ag^I_2Ag^{II}F_4$ and $Ag^IAg^{II}F_3$, J. Am. Chem. Soc. 146 (44) (2024) 30510–30517, https://doi.org/10.1021/jacs.4c11772.

[48] Rigaku OD, CrysAlisPro, Rigaku Corporation, Wrocław, Poland, 2025.

[49] B.H. Toby, R.B. Von Dreele, *GSAS-II*: the genesis of a modern open-source all purpose crystallography software package, J. Appl. Crystallogr. 46 (2) (2013) 544–549, https://doi.org/10.1107/S0021889813003531.

[50] S. Alvarez, A cartography of the van der Waals territories, Dalton Trans. 42 (2013) 8617–8636, https://doi.org/10.1039/C3DT50599E.

[51] I.D. Brown, D. Altermatt, Bond-valence parameters obtained from a systematic analysis of the Inorganic Crystal Structure Database, Acta Crystallogr. B41 (1985) 244–247, https://doi.org/10.1107/S0108768185002063.

[52] J.H. Holloway, R.D. Peacock, R.W.H. Small, The crystal structure of ruthenium pentafluoride, J. Chem. Soc. (1964) 644–648, https://doi.org/10.1039/JR9640000644.

[53] B.K. Morrell, A. Zalkin, A. Tressaud, N. Bartlett, Crystal structure of rhodium pentafluoride, Inorg. Chem. 12 (11) (1973) 2640–2644, https://doi.org/10.1021/ic50129a029.

[54] I.M. Shlyapnikov, E.A. Goreshnik, Z. Mazej, The cubic $[Ti_8F_{36}]^{4-}$ anion found in the crystal structures of $K_4Ti_8F_{36}{\cdot}8HF$ and $Rb_4Ti_8F_{36}{\cdot}6HF$, Chem. Commun. 49 (2013) 2703–2705, https://doi.org/10.1039/C3CC40756J.

[55] K. Motaln, M. Virant, M. Lozinšek, Coordination of XeF_2 to fluoridometal cations: the adduct cations $[PtF_3(XeF_2)_3]^+$ and $[PdF_3(XeF_2)_3]^+$, Inorg. Chem. 65 (10) (2026) 5668–5677, https://doi.org/10.1021/acs.inorgchem.5c05940.

[56] K.O. Christe, C.J. Schack, Synthesis and characterization of $(NF_4)_2TiF_6$ and of higher NF_4^+ and Cs^+ poly(perfluorotitanate(IV)) salts, Inorg. Chem. 16 (2) (1977) 353–359, https://doi.org/10.1021/ic50168a026.

[57] K. Radan, E. Goreshnik, B. Žemva, Xenon(II) polyfluoridotitanates(IV): synthesis and structural characterization of $[Xe_2F_3]^+$ and $[XeF]^+$ salts, Angew. Chem. Int. Ed. 53 (50) (2014) 13715–13719, https://doi.org/10.1002/anie.201406404.

[58] A.M. Heyns, C.W.F.T. Pistorius, Vibrational spectra, high-pressure polymorphism and force constants of $KAsF_6$, Spectrochim. Acta, Part A 31 (9) (1975) 1293–1301, https://doi.org/10.1016/0584-8539(75)80186-3.

[59] Z. Mazej, Polyanion condensation in inorganic and hybrid fluoridometallates (IV) of octahedrally coordinated Ti, Zr, Hf, V, Cr, W, Mn, Ge, Sn, and Pb, Molecules 29 (6) (2024) 1361, https://doi.org/10.3390/molecules29061361.